

The large size straw drift chambers of the COMPASS experiment

V.N. Bychkov^a, N. Dedek^b, W. Dünneweber^b, M. Faessler^b, H. Fischer^c, J. Franz^c,
R. Geyer^{b,*}, Yu.V. Gousakov^a, A. Grünemaier^c, F.H. Heinsius^c, C. Ilgner^{b,1},
I.M. Ivanchenko^a, G.D. Kekelidze^a, K. Königsmann^c, V.V. Livinski^a, V.M. Lysan^a,
J. Marzec^d, D.A. Matveev^a, S.V. Mishin^a, V.V. Mialkovski^a, E.A. Novikov^a,
V.D. Peshekhonov^a, K. Platzer^b, M. Sans^{b,2}, Th. Schmidt^c, V.I. Shokin^a, A.N. Sissakian^a,
K.S. Viriasov^a, U. Wiedner^{b,3}, K. Zaremba^d, I.A. Zhukov^a, Yu.L. Zlobin^a, A. Zvyagin^b

^aJoint Institute for Nuclear Research (JINR), 141980 Dubna, Moscow Region, Russia

^bLudwig-Maximilians-Universität München, Department für Physik, 80799 München, Germany

^cUniversität Freiburg, Physikalisches Institut, 79104 Freiburg, Germany

^dWarsaw University of Technology, Institute of Radioelectronics, 00-665 Warsaw, Poland

Received 12 September 2005; accepted 10 October 2005

Available online 10 November 2005

Abstract

Straw drift chambers are used for the Large Area Tracking (LAT) of the Common Muon and Proton Apparatus for Structure and Spectroscopy (COMPASS) at CERN. An active area of 130 m² in total is covered by 12 440 straw tubes, which are arranged in 15 double layers. The design has been optimized with respect to spatial resolution, rate capability, low material budget and compactness of the detectors. Mechanical and electrical design considerations of the chambers are discussed as well as new production techniques. The mechanical precision of the chambers has been determined using a CCD X-ray scanning apparatus. Results about the performance during data taking in COMPASS are described.

© 2005 Elsevier B.V. All rights reserved.

PACS: 29.40.Gx; 41.50.+h

Keywords: COMPASS; Straw drift chambers; Straw tube; X-ray; Aging

1. Introduction

The Common Muon and Proton Apparatus for Structure and Spectroscopy (COMPASS) [1] is a large aperture, high rate spectrometer, set up at the CERN Super Proton Synchrotron SPS to study the spin structure of nucleons using a polarized muon beam, interacting in a polarized target. In particular, the process of photon gluon fusion

into a charm-anticharm quark pair, which fragments to $D + \bar{D}$ mesons, is used to measure the contribution of gluons to the nucleon spin. Moreover, hadron beams are used to study the production of charmed baryons, of “exotic” hadrons (hybrids and glueballs) and to measure the polarizability of hadrons.

The setup of COMPASS, as it was in 2004, is shown in Fig. 1. The detection of particles over a large acceptance and a large momentum range requires the use of a two-stage spectrometer. The 15 double layers of large area straw drift chambers, which are described here, are used for tracking and momentum determination of charged particles produced at large scattering angles (15–200 mrad). The chambers are grouped together in five modules. Each module contains three double layers with vertical, hor-

*Corresponding author. Tel.: +41 22 767 6437; fax: +41 22 767 7910.

E-mail address: Reiner.Geyer@cern.ch (R. Geyer).

¹Present address: CERN, Dept. TS-LEA, 1211 Geneva 23, Switzerland.

²Present address: Institut universitaire de radiophysique appliquée, Grand-Pré 1, 1007 Lausanne, Switzerland.

³Present address: Uppsala University, Department of Radiation Sciences, Box 535, SE-75121 Uppsala, Sweden.

horizontal and inclined straw tubes and measures one space point. The inclined double layers are rotated by 10° with respect to the vertical ones. The chambers with vertical and inclined straws are of the same type (called type X), while the chambers with horizontal straws have a slightly different geometry (type Y). The exact dimensions of both types are given in Table 1.

In the following, the detailed dimensions refer to the type X chambers with vertical wires, which measure horizontal coordinates. A schematic view of a double layer is shown in Fig. 2. Each chamber consists of two layers of thin-film drift tubes (straws) of a length of 3202 mm which are mounted into an Al-frame. The area, covered by each double layer, is about 9 m². The straws of one layer are glued together to one plane. Every plane is divided into three sections. The central part (section B, see Fig. 2), being closer to the beam axis, is exposed to higher rates. This part is made of 254 straws with 6.144 mm outer diameter while the outer two parts (section A and C) have 96 straws each with 9.654 mm outer diameter. The chosen diameters are a compromise between minimizing the number of channels

and production cost while keeping the occupancy in each tube below 2% at maximum beam rates. The intensities, required at COMPASS, are 2×10^8 muons and up to 4×10^7 hadrons per 5.1 s spill for muon and hadron beams, respectively. A fast counting gas has to be used (Ar/CO₂/CF₄, 74:6:20).

The anode wires of the drift tubes are centered in the straws by two end-plugs and four small plastic pieces (spacers). The diameter of these gold-plated tungsten wires is 30 μm. The straws are supplied with the counting gas through the end-plugs and a gas-manifold, which is integrated into the Al-frame construction.

A thickness of only 40 mm along the beam direction was allowed for one double layer, so that three modules, containing 15 double layers in total, would fit in a volume with a length of less than 1 m between the first spectrometer magnet SM1 and the RICH detector of COMPASS. Thus, a large acceptance at a tolerable transverse size for the first stage of the spectrometer could be achieved by minimizing the thickness of the detectors.

The amount of material in the active part of the detector was optimized with respect to scattering and secondary interactions. The central part of the detector has a rectangular hole of about 20 × 10 cm² for the beam.

The required spatial resolution per double layer is 200 μm at a detection efficiency larger than 99%. The internal mechanical precision of each double layer has been required to be (or to be known) better than 100 μm.

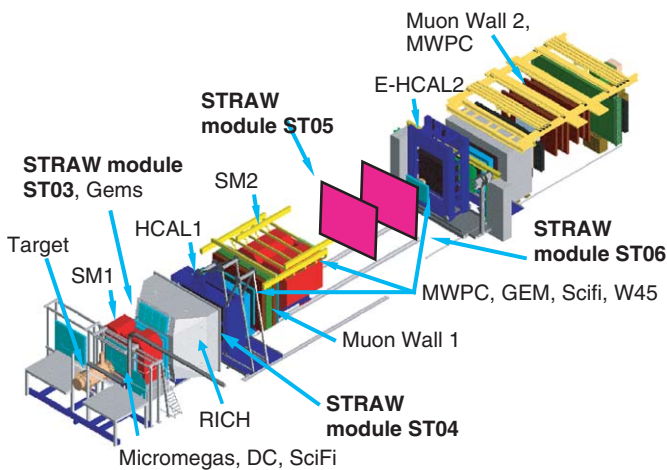


Fig. 1. The COMPASS two stage spectrometer. The straw chambers are placed directly behind the first spectrometer magnet SM1 (ST03), behind the Rich detector (ST04) and behind the second spectrometer magnet SM2 (ST05, ST06). The shown setup, which was used during the years 2002–2004, differs from the originally planned, where all chambers were to be positioned directly behind SM1.

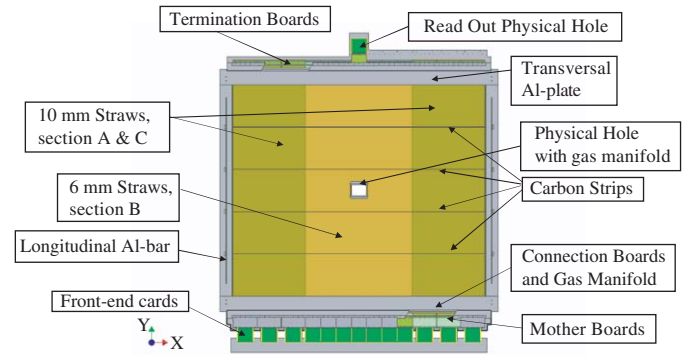


Fig. 2. Schematic view of a chamber (type X).

Table 1
Sizes and number of straws of the different double layers

| Type | Sensitive area (mm × mm) | Length of straws (mm) | Number of straws with different outer diameter | | Number of readout channels | Overall dimensions (mm × mm) |
|------|--------------------------|-----------------------|------------------------------------------------|----------|----------------------------|------------------------------|
| | | | 6.144 mm | 9.654 mm | | |
| X | 2802 × 3232 | 3202 | 380 | 384 | 892 | 4117 × 3570 |
| | | 1523 | 128 | 128 | | |
| Y | 3254 × 2427 | 3652 | 320 | 256 | 704 | 4567 × 3160 |
| | | 1752 | 128 | 128 | | |

The inclined layers are from type X too, but are rotated by 10°.

2. The straw tubes

Fig. 3 shows the structure of a straw tube. The tubes were produced by Lamina Dielectrics Ltd., Billingshurst, UK. The inner layer consists of a Carbon loaded Kapton 160 XC 370 foil from DUPONT, Wilmington, USA. It has a thickness of $40\ \mu\text{m} \pm 10\%$ (data sheet DuPont) and a resistance of $370\ \Omega/\text{square}$. This layer is glued onto a Kapton foil of a thickness of $12\ \mu\text{m}$ and aluminized ($500\ \text{\AA}$) on one side; it has a resistance of about $1\ \Omega/\text{square}$. Plastic foils have the advantage of low density and good mechanical stability at low thickness. Kapton XC, being a relatively new material, is intrinsically conductive, which makes the straws more stable against discharges and sparking. Alternative solutions had been considered: Metalized films suffer from the fragility of their thin metal layers (thickness typically a few $100\ \text{\AA}$). Carbon coated Kapton ($2K_{\text{Coated-C}}$) straws with an inner and outer graphite cover, similar to those in the ATLAS TRT [2], were tested in prototypes [3]. Problems were encountered when spacers (plastic pieces, which center the wires inside the tubes) were inserted into the straws. Carbon dust fell of the walls into the tube. For these reasons, Kapton XC was the preferred choice of material in this design.

The tolerance of the diameter of straws was specified to $-0\ +30\ \mu\text{m}$. Smaller values were not accepted by the tube producer, mainly because of the tolerance in the thickness of the foils, which were $\pm 10\%$. This already corresponds to $-0\ +24\ \mu\text{m}$.

2.1. Electrical properties of the straw tubes

The cathodes of the straw tubes have a relatively high resistance ($\rho_0 \approx 0.85\ \Omega/\text{square}$). Therefore, the cathodes are to a certain extent transparent for electromagnetic fields. This has impacts on the signal attenuation, on cross talk effects between adjacent straw tubes and on electromagnetic interferences (EMI) from external noise sources. Therefore, the electrical properties of the straw tubes were analyzed during the detector design stage. The straw tubes

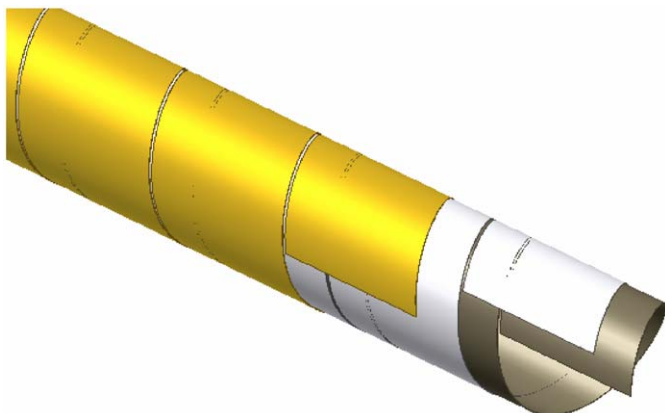


Fig. 3. Straw tube consisting of an inner layer of Kapton XC ($40\ \mu\text{m}$), glue film ($7\ \mu\text{m}$) and an outer layer of aluminized Kapton ($12\ \mu\text{m}$).

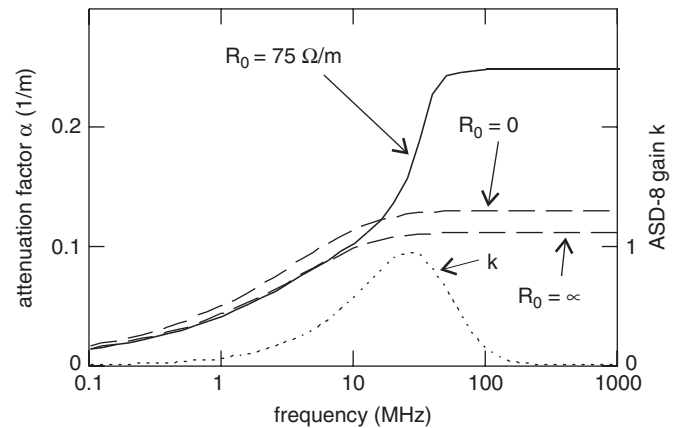


Fig. 4. The calculated attenuation factor α for the signal transmission in the 6 mm straw tube, with the $30\ \mu\text{m}$ tungsten anode ($83\ \Omega/\text{m}$) and cathode resistance $R_0 \approx 75\ \Omega/\text{m}$. For comparison, the attenuation for a zero cathode resistance (classical lossy transmission line model) and for the infinite cathode resistance is shown. The dotted line shows the gain-characteristic of the readout amplifier (ASD-8B), which defines the relevant frequency range.

were experimentally investigated [4] and modeled as a so-called double transmission line [5–7]. A straw tube is built up from a chain of elementary units. Each unit describes the resistance and inductance of a part of the anode wire and the anode–cathode capacitance. In contrast to simpler descriptions like the “lossy transmission line model”, the “double line model” takes also into account the cathode resistance and the capacity between the anode wire and the external ground.

Fig. 4 shows the results of the calculations for the frequency dependence of the attenuation factor α , which characterizes the attenuation of a signal propagating along a straw tube. For a cathode resistance of $R_0 \approx 75\ \Omega/\text{m}$ (6 mm straw), an increase of α for high frequencies (i.e. at the upper part of the frequency range of the read-out amplifiers) is observed. As a consequence, both the pulse rise time and the attenuation of the signal are slightly larger (both about 5%) than those of tubes with low resistances. The signal attenuation along the straw is not anymore exponential (Fig. 5).

The effect on the cross-talk between the straws was estimated and the result is shown in Fig. 6. The cross-talk pulse has a polarity opposite to the pulses coming from the particle detection [7]. Therefore, only the amplitude of the positive overshoot of the cross-talk pulse is relevant. Quantitatively, the cross-talk was overestimated compared to the values actually measured [8]. Both, a ^{55}Fe source and a pulse generator were used to investigate the cross-talk experimentally. The results are given in Table 2. The cross-talk between neighboring straws is typically about 0.5% and does not limit the full readout chain.

The cathode material was shown to have too large a resistance for an effective shielding against external electromagnetic noise sources. Fig. 7 shows the modulus of the cathode impedance as a function of frequency. The

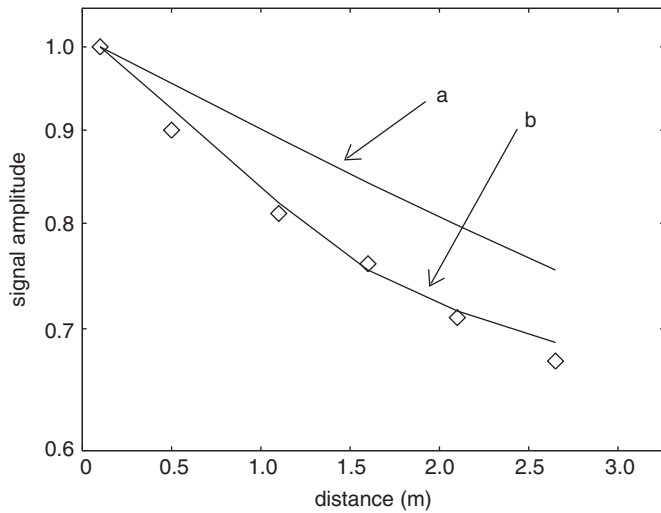


Fig. 5. Measured signal attenuation in the 6 mm diameter straw tube, 3.26 m long, with the 30 μm tungsten anode. Line a—lossy transmission line model (anode resistance 83 Ω/m), curve b—“double line” model (anode resistance 83 Ω/m, cathode resistance 75 Ω/m), squares—experimental results.

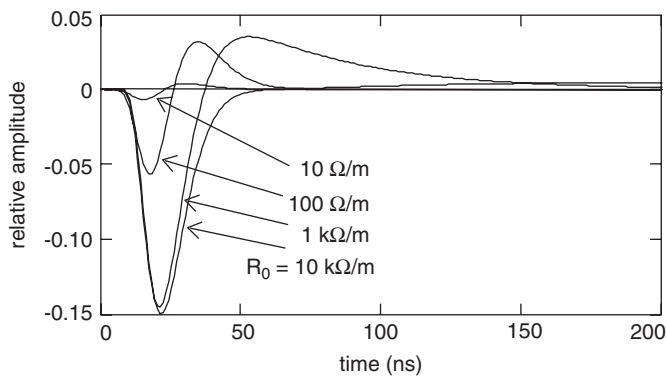


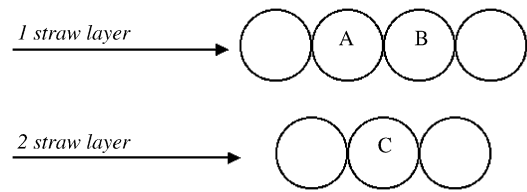
Fig. 6. Relative amplitude of the cross-talk pulses obtained from calculations for $R_0 = 10 \Omega/m$, $100 \Omega/m$, $1 \text{ k}\Omega/m$ and $10 \text{ k}\Omega/m$, where the nominal $R_0 = 75 \Omega/m$.

boundary impedance, for which the straw becomes transparent for EMI, is indicated by a dashed line. In order to improve the shielding properties, the outer detector windows of every module have been covered by an additional polyester-aluminum foil laminate. Both layers of the laminate have a thickness of 12 μm.

2.2. Aging aspects

Because Kapton XC is a new material, its radiation hardness properties had to be tested before its approval as a straw component. It was suspected, that Carbon clusters, which are responsible for the conductivity of Kapton XC, might get electrically disconnected from each other by irradiation. This could lead to local inefficiencies of the detector, an increased dark current or even sparking. In addition, radiation induced deposits on the anode wires are generally a concern.

Table 2
Measurement of the cross-talk of neighboring channels



| Straw diameter (mm) | Scheme of measurement | Cross-talk vaule (%) | | | |
|---------------------|-----------------------|----------------------|------|-------|-------|
| | | MB | TB | Straw | Total |
| 9.56 | A–B | 0.33 | 0.45 | 0.42 | 1.2 |
| | A–C | 0.94 | 0.51 | 0.29 | 1.76 |
| 6.03 | A–B | 0.44 | 0.40 | 0.66 | 1.5 |
| | A–C | 1.1 | 0.55 | 0.41 | 2.05 |

The contribution of straws and parts of the readout chain (motherboards (MB) and termination boards (TB), see also Section 3.5) are listed separately.

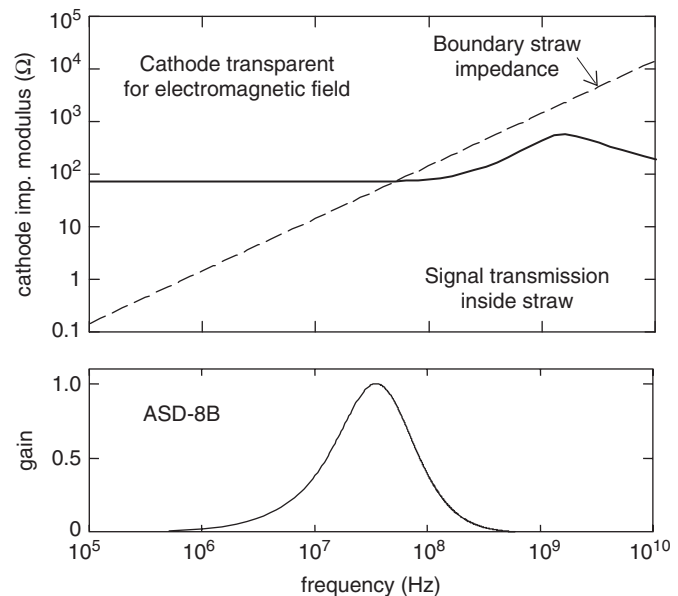


Fig. 7. Top: modulus of the cathode impedance (6 mm straw tubes). The dotted line shows the boundary impedance value, for which the cathode becomes transparent for electromagnetic fields (which manifests itself by the rapid change of the straw transmission line characteristic impedance). Bottom: the frequency characteristic of the readout chip (ASD-8B) for comparison.

The goal of the measurement was to test the radiation hardness of the overall detector design in connection with the chosen gas mixture Ar/CO₂/CF₄ (74:6:20). The aging properties of straws were studied with 26 MeV proton beams from the Munich Tandem accelerator [9]. Charge doses of 1.1 C/cm were accumulated in each of two samples of straw prototypes. These doses correspond to the estimated radiation load on the innermost anode wire sections induced by the beam halo in 4 years of COMPASS

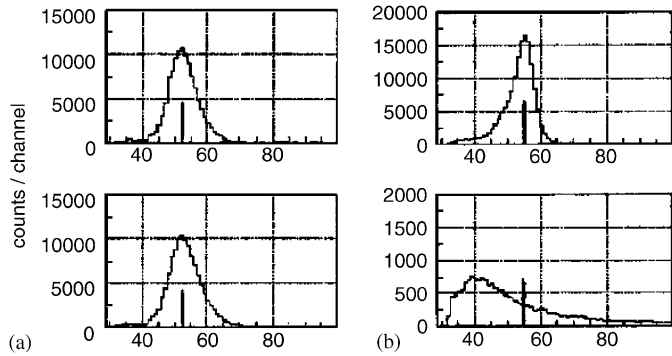


Fig. 8. Gas gains before (top) and after (bottom) the irradiation for a) Ar/CO₂/CF₄ (74:6:20) and for b) Ar/CH₄ (90:10).

operation at a gas gain of 10^5 . Two independent experiments, yielding consistent results, were carried out.

To achieve these doses in the proton test experiments, each of 4 days duration, rather large fluxes of $(2\text{--}4) \times 10^6$ protons/mm² were required. However, care was taken to keep the gas gain at realistic values, despite the space charge effects associated with the large fluxes. This was achieved by increasing the applied voltage by 200–400 V above the nominal values, such that the monitored gas gain maintained the nominal value. The accumulated charge was measured with a current integrator. The dependence of the gas gain on the accumulated charge dose was investigated with high sensitivity in beam-off periods, using 5.9 keV X-rays from a ⁵⁵Fe source. As demonstrated by the pulse height spectra shown in Fig. 8a, no significant peak shifts occurred after irradiation. As an upper limit, corresponding to two standard deviations, a relative loss in gas gain of 1% is extracted from both experiments with 1.1 C/cm total charge dose.

For comparison with the gas mixture chosen by the COMPASS experiment, one straw detector was filled with Ar/CH₄ (90:10) in one of the irradiation experiments. As apparent from Fig. 8b, the gas gain drops dramatically after application of the proton radiation dose. A relative loss of 23% for 1.1 C/cm charge dose is extracted from these data, which compares well with other tests of Ar/CH₄. Another well-known aging effect is the so-called Malter current, which is attributed to field emission of electrons through deposits on the cathode, built up during irradiation [10]. This effect leads to an increase of the anode current during irradiation with a constant flux and of the dark current, when the beam is switched off. Both phenomena were clearly observed with the Ar/CH₄ mixture [9]. With the (Ar/CO₂/CF₄) gas mixture, however, no indication of increased currents due to Malter effect or any other reason were found after application of the 1.1 C/cm charge dose.

Direct searches for surface deposits in the irradiated detectors were performed with a scanning electron microscope (SEM) and an elastic recoil detection analysis (ERDA) with 200 MeV Au ions. Needles and droplets with extensions of 10–20 μm were observed on the anode

wire and on the cathode in the irradiated section of the straw detector operating with Ar/CH₄. In straws operating with the (Ar/CO₂/CF₄) gas, however, only a thin scaly deposit of less than 0.1 μm thickness was found on the anode wire in the irradiated section. In general, swelling of the anode wire causes a loss of gain at given voltage. The upper limit of 0.1 μm for a wire of 30 μm diameter is, however, consistent with the above upper limit for the loss of gain and, hence, can be tolerated. As revealed by ERDA, the relative abundances of the elements C, N and Si are increased in the deposit in comparison with the wire surface in a non-irradiated section. Straw detectors engaged in the COMPASS experiment since 2001 have accumulated charge doses of up to 0.2 C/cm in the inner section and do not show signatures of aging so far.

2.3. Mechanical properties of the straw tubes

The high absolute precision, required for these large area chambers, and, at the same time, the need to minimize the amount of material in the active part of the detector, necessitated a detailed understanding of the basic material properties. The plastic foils used for the straw tubes are hygroscopic. Thus, production and operation of the detectors must take place under controlled humidity. Both the Al-frame and the Kapton straw tubes have relatively large temperature expansion coefficients. Furthermore, the straw tubes have to be sufficiently gas tight. The plastic materials have to be adhesive to commercially available glues.

The difference in expansion coefficients $\Delta\alpha$ for Al and Kapton ($\alpha = 23.2 \times 10^{-6}$ and $18 \times 10^{-6} \text{ K}^{-1}$, respectively) lead either to an increase in tension of the straw walls or to a bending of the straw planes with temperature changes. For a straight straw of length L , being not under mechanical tension, the sagitta S caused by a temperature decrease ΔT can be estimated by the following expression:

$$S/L = \sqrt{\frac{1}{3}\Delta\alpha\Delta T}.$$

For $L = 3.2$ m, a 1 K temperature decrease would result in a sagitta of 4 mm. In our case, this value decreases to 0.8 mm as we are using four orthogonal carbon strips, which give additional support to the structure. In addition, an increasing temperature leads to an expansion of the transversal Al-plates of the frames. Consequently, that part of the straw plane, which is located between these Al plates and the next neighboring carbon strips, also expands orthogonally to the straw axis. The change of the overall plane width near the Al rods is about 75 μm per K (assuming a width of 3.2 m).

In order to estimate the value of elongation with increasing humidity, straws made from three different materials were placed into a climate box. The first straw sample consisted of the material used for the detectors described in this paper: Carbon Loaded Kapton for the inner layer and aluminized Kapton for the outer layer

($KK_{\text{Loaded-C}}$). The other two samples were made from Carbon Loaded Kapton (inner layer) and aluminized Mylar ($MK_{\text{Loaded-C}}$) or rather Carbon Coated Kapton for both layers ($2K_{\text{Coated-C}}$). The straws had a length of 3.2 m and diameters of 6.02 and 9.56 mm. Every point was measured after the material was kept for 1 day under constant humidity. The result is shown in Fig. 9. The relative elongations for a humidity change of 1% were measured to be 1.6×10^{-5} for ($2K_{\text{Coated-C}}$), 2.9×10^{-5} for ($KK_{\text{Loaded-C}}$) and 2.1×10^{-5} ($MK_{\text{Loaded-C}}$) straws. After drying, all straws returned to their original length. The time dependence of the process is shown in Fig. 10 for a

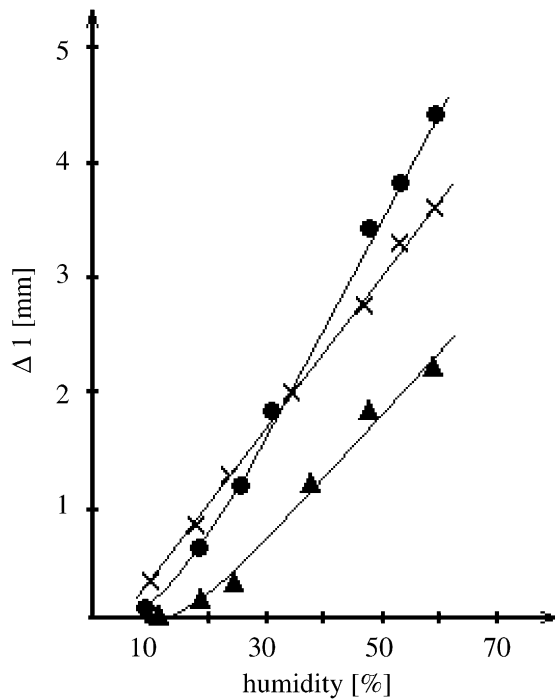


Fig. 9. The change of the length of a 3.2 m long straw as a function of the relative air humidity ((●)— $KK_{\text{Loaded-C}}$, (x)— $MK_{\text{Loaded-C}}$, (▲)— $2K_{\text{Coated-C}}$).

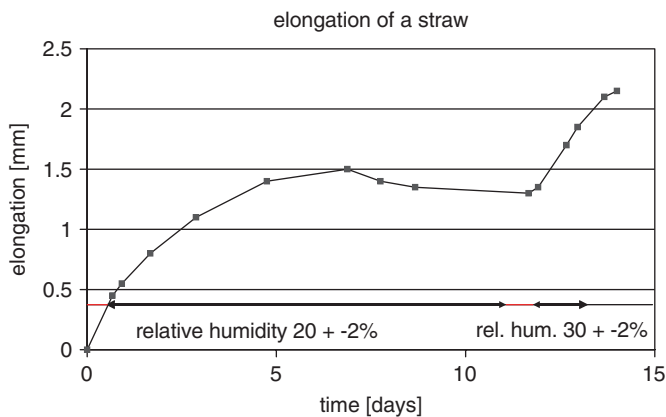


Fig. 10. Dynamical behavior of a 3.2 m long $KK_{\text{Loaded-C}}$ straw. The material was absolutely dry and then first exposed to a 20% relative humidity for 11 days and, subsequently, to 30% relative humidity. It has taken about 1 day, before the new humidity setting has stabilized to 30%.

$KK_{\text{Loaded-C}}$ straw. The water absorption takes several days, before the system reaches equilibrium.

These results show the importance of controlling the temperature and the humidity during the chamber production. The temperature should be lower and the humidity should be higher compared to the final working conditions in order to give the straws the right tension. It is partially possible to compensate the difference of working and assembly temperature/humidity by using the elasticity of the frame elements during the assembly procedure.

3. The straw chambers

The active part of each chamber consists of two layers of straws of a length of 3202 mm, which are glued together to a plane. A plane of this kind has a much higher mechanical stability compared to individual straws. This improves the ruggedness and the mechanical precision, which can be achieved. The load onto the frame, which would be needed to keep individual straws straight enough by tension, can be significantly reduced. The production technology, which is the basis for this design, will be described below.

Two straw planes are combined to one double layer and mounted into an Al-frame as shown in Fig. 11. One layer is shifted by half a diameter with respect to the other in order to resolve left–right ambiguities and to obtain efficiencies larger than 99% for at least one track coordinate. Efficiency losses, which are mainly due to the geometry, are around 6% per layer. The ends of the straws of a double layer are glued gas tight between two transversal Al-plates on each side of the frame, which serve at the same time as a part of the gas manifold (Fig. 12).

The straw layers are supported by carbon fiber strips, which are parallel to the transversal Al-frame elements. They are glued to the planes every 60 cm and are fixed to the longitudinal Al-bars of the frame.

The gas manifold is illustrated in more detail in Fig. 13. The counting gas streams through the manifold and through the end-plugs into the straws from the bottom side of the chambers and exits through the manifold on the top. The electrical connections to the anode wires are fed through the gas tight volume by connecting boards (CB). The straws are read out on the bottom side only, while they are terminated on the top by termination boards (TB). Motherboards (MB, see Section 3.5) and front-end electronics are supported by the chamber frame.

Thirty-two straws in the center of section B are cut into two and shortened, leaving a material-free hole for the

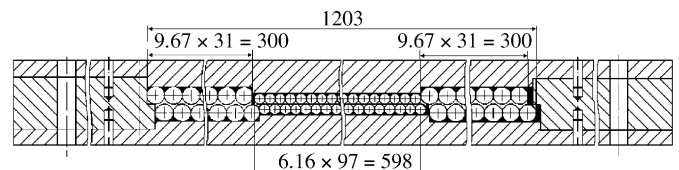


Fig. 11. Cross section of a double layer.

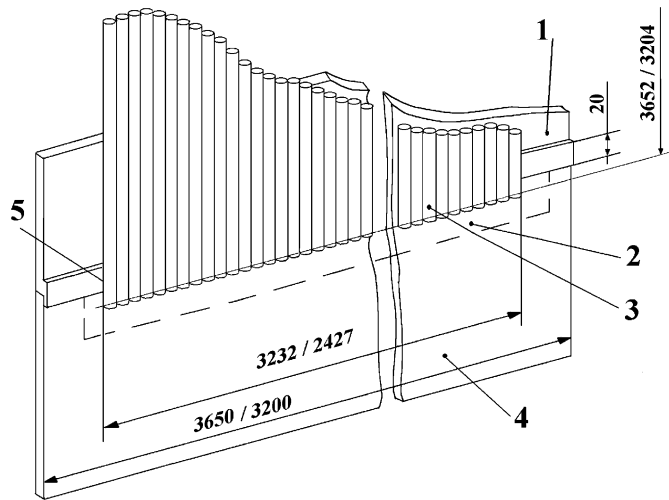


Fig. 12. The two straw-planes are sandwiched and glued gas tight between two transversal Al-plates. Only one plane and one transversal plate are shown. 1—transversal Al plate, made with an accuracy of better than 0.1 mm; 2—boundary dimensions of the chamber gas volume; 3—straw-plane; 4—Al element used to mount peripheral elements (mother boards, readout cards) of the chamber; 5—area where the straw-plane is gas tightly sealed into the Al frame.

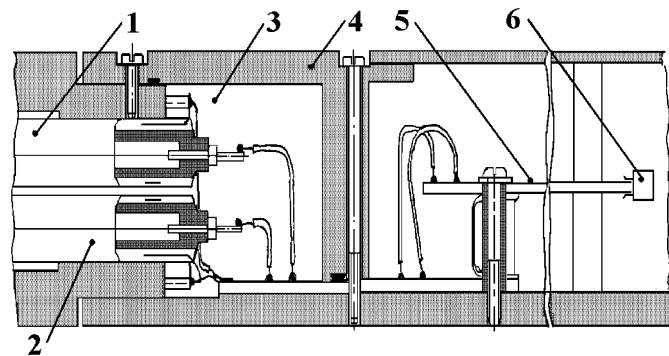


Fig. 13. A scheme of the peripheral gas volume of the chamber. 1,2—two straw-planes; 3—gas volume; 4—removable cover of the gas volume; 5—readout; 6—connector for front-end electronics.

beam of about $20 \times 10 \text{ cm}^2$. A gas manifold, which is installed close to this hole, ensures a proper gas flow. The amount of material used for this manifold has been kept at the lowest possible value, in view of the large number of secondary particles and beam halo in this region for hadron and muon beams, respectively. The shortened straws are read out by MB and front-end cards at the bottom and the top side of the chamber. They are terminated in the center.

3.1. The assembly of straw chambers

The design and assembly technology of the COMPASS straw chambers [8] are based on the experiences gained by the development of a prototype [3]. The assembly of straws into a chamber proceeds in three steps. First, straws are

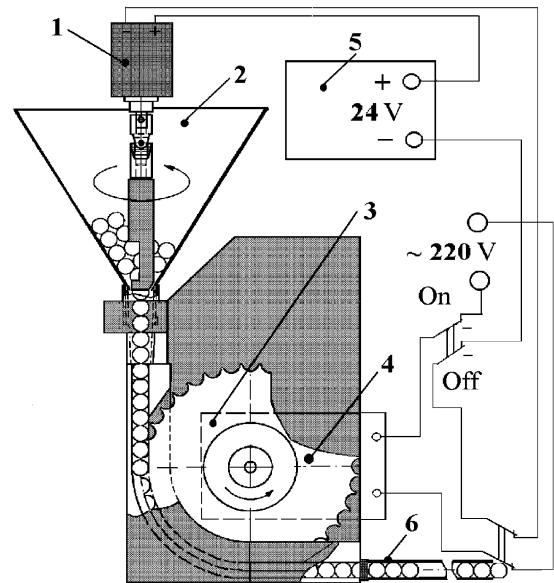


Fig. 14. Tool for filling the straw with precision balls. The mixer with engine (1) and volume (2) containing precision balls; pushing gear (3) with engine (4); power unit (5); straw (6).

glued together to form a sub plane. There are three sub planes per plane, one with 6 mm straws (section B in Fig. 2) and two with 10 mm straws (sections A and C). Then, the three sub planes are assembled to form a plane. Finally two planes are put together into one common frame.

Before gluing straws together to a sub plane, each straw is filled with precision steel balls. The balls have diameters of 6.010 ± 0.003 and 9.525 ± 0.003 mm, depending on the straw diameter. A special tool was built to insert the balls. It is shown in Fig. 14. The filling of one straw of 3.6 m length takes about 2 min. A sub plane is assembled on a precision table. Every straw is aligned to its final position with a precision ruler. After all straws of a sub plane were aligned, neighboring straws were glued together. Ruetadur SL/Ruetapox L20 (Bakelite AG, Iserlohn, Germany) glue was used. The amount of glue was kept below 60% of the weight of the straws. Fig. 15 shows the precision table with a straw plane and an automat for gluing. The width of a sub plane is preserved by four carbon fiber strips, 0.5 mm thin and 9 mm wide, which are glued, at equal distances, orthogonally to the straws. Finally, the balls are removed. The precision of positioning each straw in a sub plane depends on the accuracy of plastic rods used as plug elements and also on the precision of straw diameters: it is within 0.1 mm.

In the second assembly step, three sub planes (a central one with 6.02 mm diameter straws, and two outer ones with 9.53 mm straws) are mounted into a common straw-plane. A large precision table is used.

As already shown in Fig. 12, the completed straw plane is gas tightly glued to the two transversal Al plates of the frame. Araldite 2011 and epoxy glues BK-9 and ALK-5 [11] are used to glue the planes. Then, the two single layers

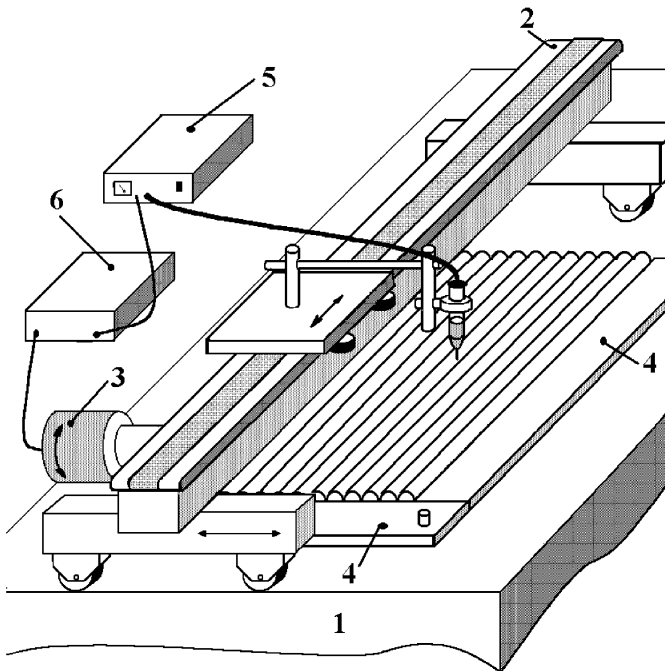


Fig. 15. Automat for gluing straws to a sub plane. Precision table (1); linear module (2) with engine (3) used to move a syringe with glue along the straws; precision rulers (4); glue dispenser (5); control unit (6).

are assembled to one double layer by connecting them to the two longitudinal Al bars. At this stage, the chamber is prepared for installation of the anode wires into the straws.

3.2. Internal straw elements

A gold-plated tungsten wire with $30\ \mu\text{m}$ diameter (type 861, LUMA-METALL AB, Kalmar, Sweden) is used as anode. The wire tension was set to 90 g, close to the elastic limit which is around 120 g, as shown in Fig. 16. Polycarbonate end-plugs, produced by applying the method of pressure molding, are used to fix the wires at the ends of the straws (Fig. 17A). The diameters of the end-plugs are $9.5(+0; -0.022)$ and $6.0(+0; -0.018)$ mm, depending on the corresponding straw diameters. There are two grooves on the outer surface of the end-plug, which connects the internal straw volume to the gas manifold, which is common to all straws. A contact spring is inserted into a gutter of the end-plugs. The spring pushes against the inner wall of the straws and electrically connects the cathode with the common ground of the chamber. Around the physical hole, slightly different weight optimized end-plugs are used.

In order to decrease any displacements of a wire due to electrostatic and gravitational forces, four spacers are glued at equal distances to every wire, before the wire is inserted into the straw. Fig. 17B shows a sketch of a spacer. The spacers are produced of polycarbonate by pressure molding. Their design is optimized in order to reduce their mass, which is only 25 mg for the spacers with $9.49(+0,$

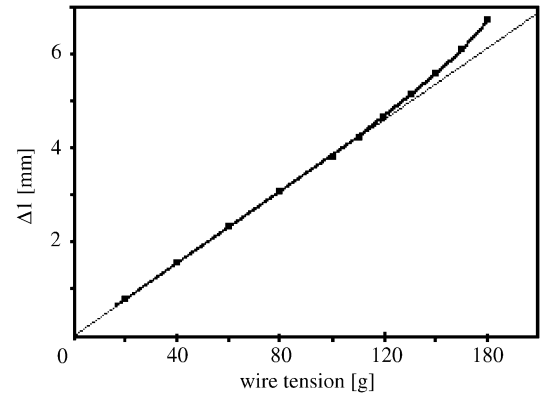


Fig. 16. Elongation of a 1 m long wire as a function of the applied weight in units of gram.

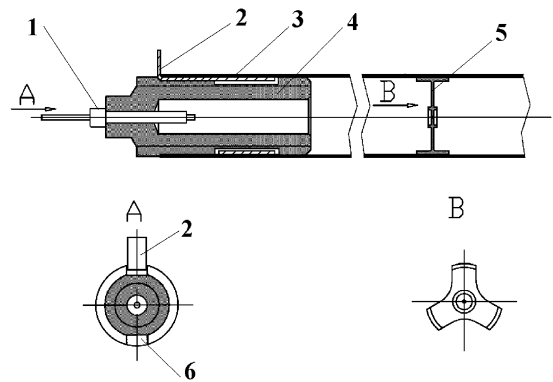


Fig. 17. Scheme of a straw (3) with an inserted end-plug (4) and a spacer (5). Crimp Pin (1) for fixing an anode wire, ring spring (2) for grounding the straw cathode, gas channel (6). (A) Top view of an end plug. (B) Top view of a spacer.

$-0.022)$ mm and 15 mg for the spacers $5.97(+0, -0.018)$ mm diameter. To reduce the insensitive zone in the vicinity of the spacers, their dimensions are minimized as well. The spacers are fixed with droplets of Araldite 2013 glue. A special support structure guarantees the precise position of the spacers during the gluing process.

During the process of wiring, the straw chambers are put to a vertical position. The wires are led through the top end-plugs, to which they are fixed by the crimp pins [12,13]. Then the wires and spacers are inserted into the straws from the top. Subsequently, the bottom end-plugs and crimp pins are installed. After the wire tension has been adjusted, the wires are fixed on the bottom end-plugs again by crimping. The tension of each wire was measured after the installation through the wire resonance frequency. A typical distribution of the measured tension is given in Fig. 18. The tension is within 90 ± 10 g for approximately 95% wires and within 90 ± 15 g for all of them. Every individual wire of all chambers was again controlled after the complete assembly and electrical soldering of a chamber. A total of 2–3% of anode wires had to be replaced because they were broken or the spacers were misplaced.

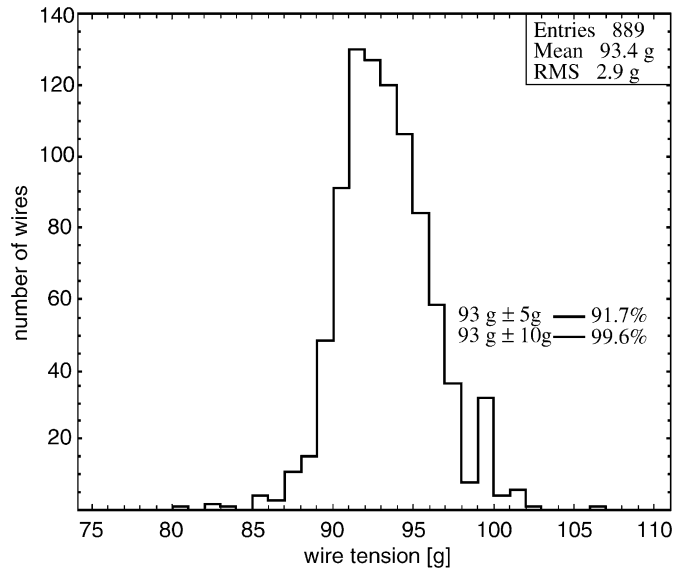


Fig. 18. A typical distribution of the wire tension for 889 straws of a double layer.

3.3. The physical hole

The central part of the chamber, where the particle flux is very high, has to be insensitive. A central hole of $126 \times 194 \text{ mm}^2$ area (physical hole) was cut out of each chamber. Thus, the inner part of the two inner sub planes (6 mm straws) of a double layer, which contains the physical hole, consists of pairs of short straws ending at the border of the physical hole. They are connected to separate readout channels. This has the advantage of reducing the occupancy by a factor two in this region of highest occupancy. Having a hole, instead of simply deactivating the wires, was preferable in order to reduce the material in the path of the beam and beam halo and thus to reduce secondary reactions of the beam outside the target.

The end of the straws, which is close to the physical hole, is electrically terminated. Here, special, light polycarbonate end-plugs (Fig. 19) and crimp pins are used to fix the wires. Thin-walled (0.1 mm) metal tubes are glued into the end-plugs, which connect the straws to a gas manifold. Each plane of a chamber has two of these “low mass” manifolds. They are made from fiber-glass laminate with a thickness of 2 mm. Manifolds have a size of $230 \times 15 \times 9 \text{ mm}^3$. The two manifolds at the physical hole of a plane are connected to each other with two tubes made from plastic films. The structure is self-supporting. The gas manifold is carried by the metal tubes, which connects the straws inner volume to the manifold itself.

The material price to pay for the physical hole is additional matter, located in the “frame” zone around the physical hole with an area of $126 \times 194 \text{ mm}^2$. The radiation thickness in this chamber zone is $2.0\% X_0$, whereas the radiation thickness of the normal sensitive area is $0.2\% X_0$

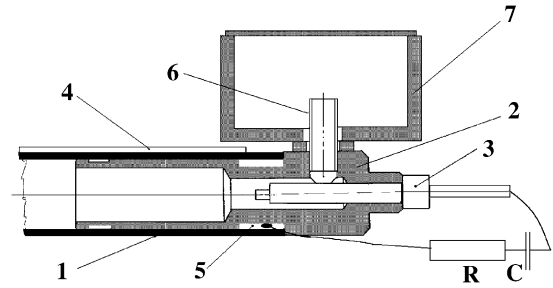


Fig. 19. Inner end of a straw (1) facing the physical hole. End-plug (2) with crimp pin (3); fiber glass frame (4), 1 mm thick with $230 \times 220 \text{ mm}^2$ outer and $200 \times 200 \text{ mm}^2$ inner dimension; ring groove (5) for hermetic straw sealing and connection of the termination RC chain to the cathode; metal tube (6); gas manifold (7).

per double layer (without taking into account the gas in the straws).

3.4. The protective volume

As already described, the length of the straw tubes is strongly affected by humidity. In order to keep the straw tubes straight, they must be kept under a small tension. Any shortening of the straw tubes by a few $100 \mu\text{m}$ would result in an increasing tension inside the straw tubes, which, at the end, would have to be held by the frame construction. Even worse, a lengthening would result in a bent of the straw planes.

In order to minimize the effects of humidity, the straw planes have to be surrounded by a dry gas. For this purpose, two protective foils were glued onto the Al-frames of every double layer, thus creating a closed volume around the straws.

The technical requirements for this “protective” volume were to keep the humidity constant and below 10%. The maximum bent of the nearly 10 m^2 protective foils must be less than 1.5 cm in order to avoid mechanical contact with other detectors. The radiation thickness of the material should be small compared to the active components of the detector.

The windows were made of Mylar foils, aluminized on both sides with a thickness of $12 \mu\text{m}$. The Mylar has a sufficient mechanical strength, while the aluminum layers are needed as a barrier against water vapor. The water vapor transmission coefficient of the foil was tested to be smaller than $0.05 \text{ g}/(\text{m}^2 \text{ day})$ at 25°C and 70% relative humidity. Most other types of thin plastic foils without metallization would have been too transparent for water vapor.

Since aluminized foils are not produced with the required width, several foils had to be glued together to a larger unit of $4 \times 3 \text{ m}^2$. With the help of a support frame, the resulting foils were stretched and then glued to the double layers.

In order to limit the bent of the windows to less than 10 mm, the difference between the gas pressure inside a protective volume and the outside atmospheric pressure is

kept on a level of a few Pa only. This small pressure difference was achieved by using exhaust pipes with a length of 300 mm and an inner diameter of 6 mm. The exhaust pipes, fixed on the top of the chambers, together with the applied gas flow, regulate the pressure differences to the outside atmosphere by their flow resistances and prevent air from diffusing back into the protective volumes. A gas flow of 30 l of Nitrogen per hour leads to a pressure drop of 1.3 Pa along the pipe. Atmospheric pressure changes due to weather conditions, which are large compared to the allowed pressure difference, are automatically buffered by the elasticity of the protective foils. Nitrogen was chosen as the protective gas, because of its similar density compared to air. The pressure difference over 3 m height due to the gravitational field is 36.17 Pa for Air and 35.05 Pa for N_2 . The 1.1 Pa difference in pressure reduces the bent of the foils. Other inert gases, like CO_2 or Argon, had to be excluded from our choice, because their densities are too different from Air. They would have led to pressure differences between the protective volume and the outer atmosphere of 13 and 18 Pa, respectively, which is one order of magnitude too large.

3.5. The electrical periphery

In order to avoid pulse reflections, an impedance matching (termination) on the far end of the straw would be sufficient. However, a termination on both ends has been favored, because capacitors (82 pF—SMD) with smaller values could be used between the straw and the termination circuits. A small capacitance reduces the risk of an anode wire break in the case of discharges in the detector. A resistor of $360\ \Omega$ terminates the straw at the far end. An additional serial resistor R_s (240 and 270 Ω , for 6 and 10 mm straws, respectively) at the amplifier input together with the input resistance of the amplifier give the right impedance for the termination on the readout side of a straw.

The 64-channel MB contains a high voltage distribution circuit, a coupling between straw tubes and amplifiers, which includes also HV protection diodes for the amplifier inputs, and a test pulse line, which can be used for the calibration of the full readout chain. The TB contain resistors and capacitors used for the impedance matching of the far end of the straws. Additional small printed circuit boards, called CB, are glued to the frame. The aim of these boards is to transmit pulses from the straws, which are filled with working gas, to the MB, which are operated in air. All printed circuit boards are produced in a multi-layer technology and they are processed with a special milling procedure in order to achieve a set of channels which are, after the board assembly, filled with epoxy resin, which protects HV elements against breakdowns.

The high-voltage distribution circuits contain two-stage RC filters, which protect the amplifier input against pick-up noise in case of a HV-trip in one of the channels. A simplified MB circuit diagram (for one channel) is shown in Fig. 20.

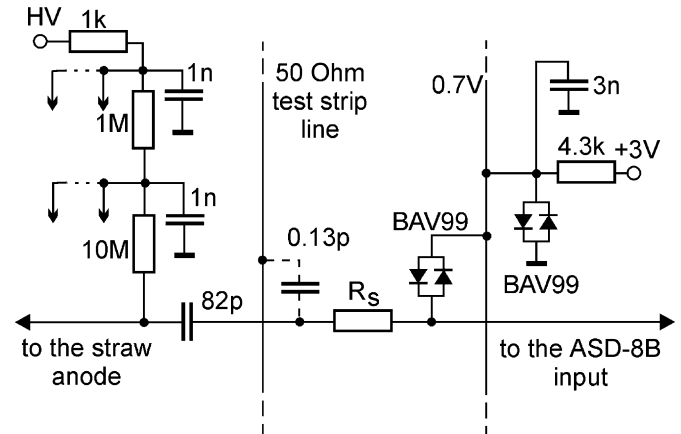


Fig. 20. Simplified circuit diagram of the Motherboard.

4. Quality control and performance of the chambers

4.1. Tests of the chambers after their production

After the assembly work is finished, a quality control is performed for every chamber. The gas leakage under normal operation of a chamber is measured. The chamber is accepted, if the leakage rate stays below 5 l/h. This number has to be compared with the size of the active gas volumes (without taking into account the volumes of the gas manifolds), which is 126 l for a type X chamber and 104 l for a type Y. The leakage of the chambers is not limited by the diffusion of the gases through the straw walls, as one would expect, but is mainly caused by small holes in the straw walls. Whether the holes were already present in the foil material before the straw production, or whether they were produced during the detector assembly is at present not understood. In this context, one specification of the straw material was found to be problematic. While 12 μm thick Kapton films were used for the outer layer, 40 μm was used for the inner layer of the straw tubes. The choice was taken in order to minimize the material budget and because of the availability of materials. Nevertheless the different thicknesses cause a mechanical fragility at the seams of the straw tube windings, which might have resulted in some holes. Only a few holes along 1 km of straw tube material can explain the observed leakage. Moreover, a leakage test of every individual straw tube before the assembly would have been preferable.

Every channel of every chamber is tested with the help of a ^{55}Fe source and a single channel amplifier. The uniformity of the gas gain is controlled and the signal attenuation is measured. While most tests on the chambers were performed at a gain of 2×10^4 , the stability of the operation of the chambers is tested at a gas gain of 10^5 . Ar/ CO_2 (80:20) was used as a test gas mixture.

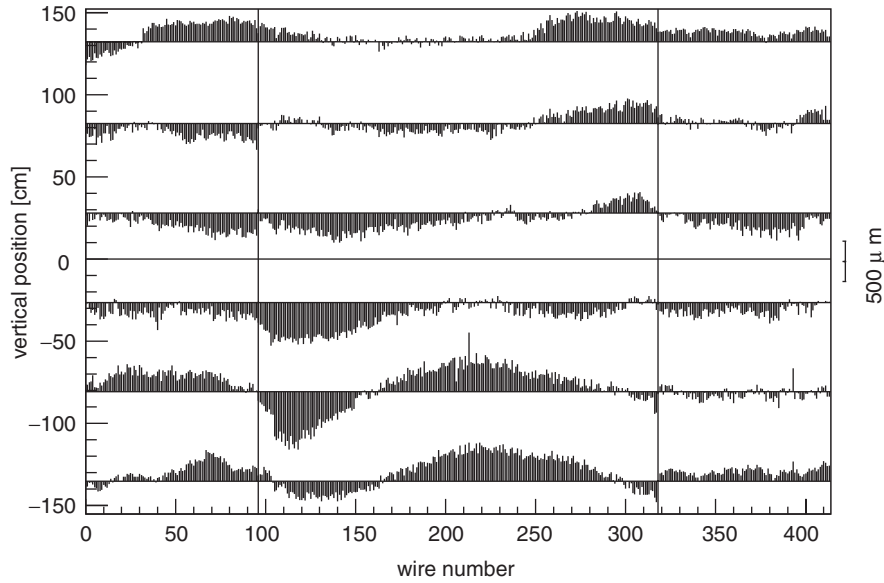


Fig. 21. Deviations of the measured wire coordinates Δx_{wi} from an ideal wire grid for a layer with vertical straws. The wires were measured at six vertical positions, two close to the upper and lower ends of the straws and four close to the spacer positions. The deviation from the ideal wire grid is indicated by the length of the lines. The scale is given on the right side.

4.2. X-ray measurements

The technical specification of the straw drift chambers in COMPASS required a spatial resolution of $200\ \mu\text{m}$ for single wires and mechanical inaccuracies below $100\ \mu\text{m}$ within the wire plane. The deviation from planarity of the wire planes should be less than $500\ \mu\text{m}$.

The resolution of a straw tube is limited by its intrinsic properties like the drift cell geometry, the gas properties, the gas gain and the readout electronics. The systematic errors of the track coordinates, on the other hand, are given by the mechanical precision of the chambers, mainly the wire positions.

An X-ray scanner was developed and built to measure the coordinates $x_{wi,X\text{-ray}}$ of every individual wire w at six positions i , at the two ends of a given straw and at the four spacer positions [14]. Thus the wire coordinates within the planes have been measured with a precision better than $40\ \mu\text{m}$. Since a method of triple stereo imaging is used, also the coordinates of the wires perpendicular to the planes are obtained with a precision of $100\ \mu\text{m}$. In total, about 75 000 coordinates had to be measured [15]. Fig. 21 shows the deviations $\Delta x_{wi} = x_{wi,X\text{-ray}} - x_{wi,\text{average}}$ of the measured coordinates from their corresponding average values $x_{wi,\text{average}}$ for one layer of a typical double layer as a function of the wire and spacer number. The average coordinates refer to an ideal wire grid, where the wires are assumed to be straight, coplanar and equidistant with a regular pitch p . Every section A, B and C of a straw layer is described by a separate grid. The parameters of every grid—the wire pitch p , the translation vector and the rotation matrix—were obtained from a fit to the measured coordinates $x_{wi,X\text{-ray}}$, where $\sum \Delta x_{wi}^2$ was minimized. The obtained values for p are plotted in Fig. 22 for all layers

and sections. These “mean” wire pitches differ by $5\text{--}10\ \mu\text{m}$, which amounts to differences of up to 2 mm on the overall size of a layer. For COMPASS, it is necessary to determine the overall size and the resulting wire pitch of every detector layer and section after the production with accuracy better than $100\ \mu\text{m}$. The real values derived from alignment runs are to be used in the offline analysis.

The distribution of all measured deviations Δx_{wi} is shown in Fig. 23. It has nearly a Gaussian shape and a width of $178\ \mu\text{m}$ (RMS). Since this value exceeds the desired upper limit of $100\ \mu\text{m}$ for the systematic errors of the track coordinates, as required by COMPASS, the individual wire coordinates must be corrected offline based on the positions obtained by the X-ray calibration. Fig. 24 shows the variances of the Δx_{wi} distributions for individual detector layers. The values vary between 100 and $250\ \mu\text{m}$. This result shows that the production quality was varying, but the technology is in principle suited to build large area detectors with an absolute wire position precision of $100\ \mu\text{m}$. To achieve this, the stability of the conditions during the production process would have to be improved.

For the same six points along the wires, which were already described, also the deviation of the wire positions perpendicular to the ideal plane has also been measured. This result for the planarity of the chambers is given in Fig. 25. The maximum deviation of all straws from the ideal plane is plotted. The non-planarity stays below $500\ \mu\text{m}$ which fulfills the COMPASS technical specification.

4.3. Reliability and performance in COMPASS

Since the departure of the chambers from the site of their production (Dubna, Russia) where all 12 440 straws were

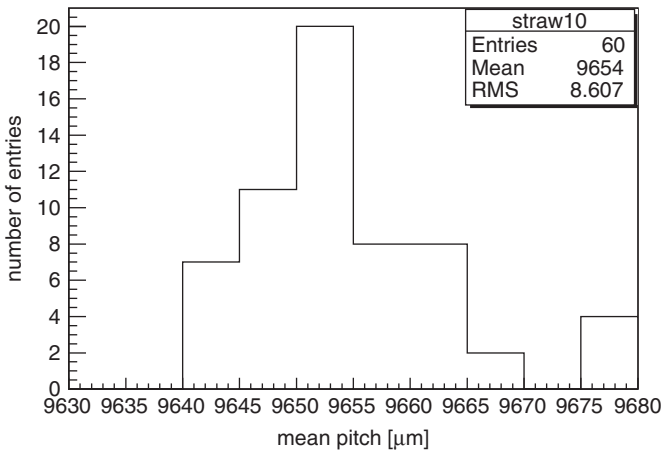
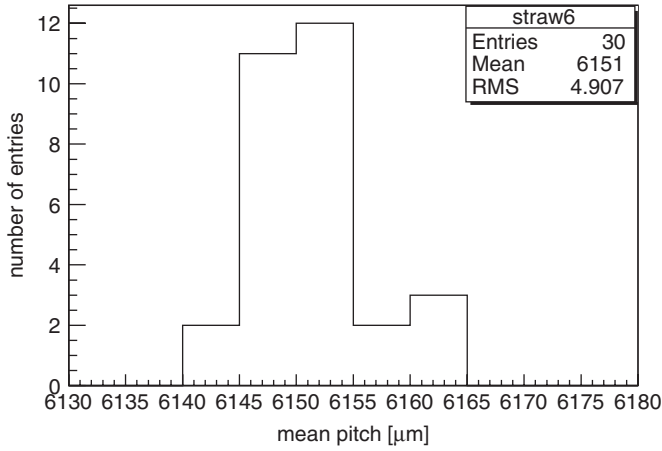


Fig. 22. Distribution of mean wire pitches for the detector sections with 6mm straws (top) and 10mm straws (bottom).

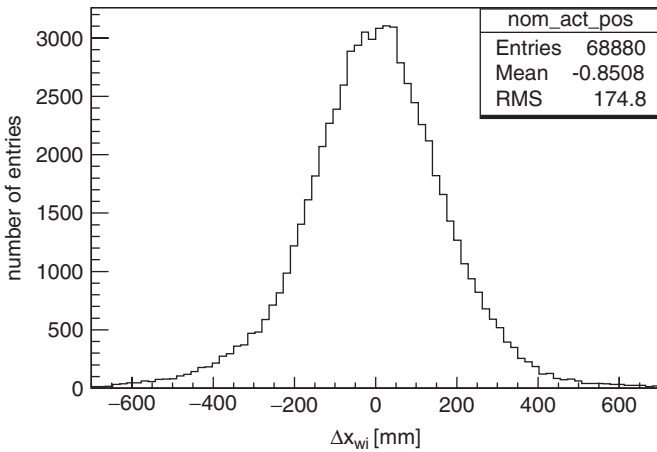


Fig. 23. Deviations of the measured wire coordinates from a perfect wire grid. The distributions include the coordinates of all wires, all chambers, measured at six positions each.

tested and operational, less than 20 straw tubes became inoperative after the transport and 2 years of operation in COMPASS. The main reasons for loosing channels were broken HV capacitors, which could be replaced, and some

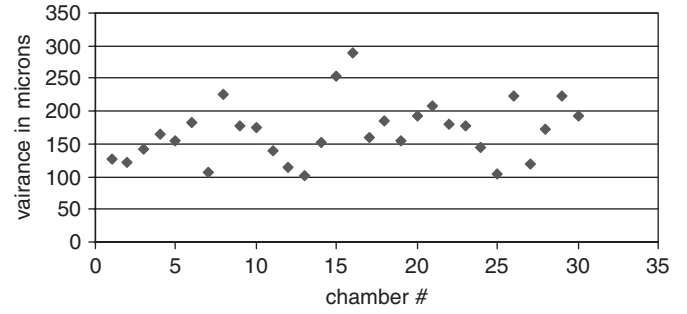


Fig. 24. The variances of the distributions of Δx_{wi} , plotted separately for all layers (sections B only).

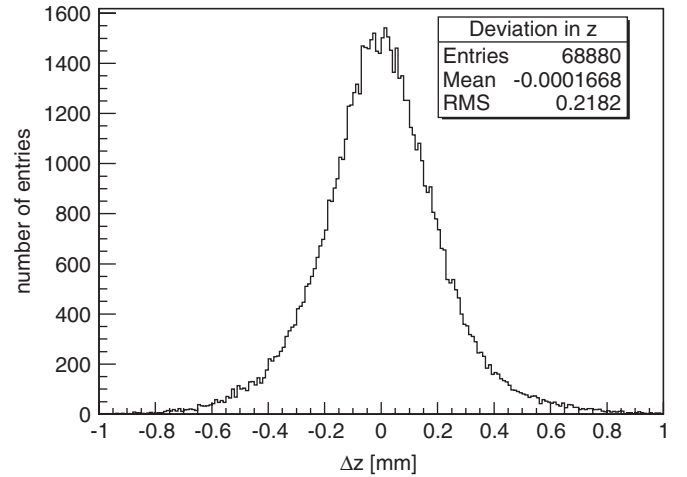


Fig. 25. Deviation from planarity. The distribution includes the coordinates of all wires of all planes, measured at six positions each.

broken wires (< 10). During the operation with beam, 187 of 200 HV channels (1 HV channel = 64 straws) worked stable at the nominal gas gain of 6×10^4 . Their mean trip probability was about one trip per card in 100 days. The current limits of the HV supplies were put to $30 \mu\text{A}$, which is about a factor of two higher than the currents introduced by the beam.

The remaining 13 channels, distributed over four chambers could not always be operated at nominal gas gain. The stability of their operation and the maximum HV, which could be applied, depends on the environmental temperature in the experimental hall. While at low temperatures, only four channels were affected, the number of unstable channels reached 13 during the hottest summer periods. The effect was reproducible.

The reason for the instabilities is a bending of the straw tubes, which, in turn, leads to badly centered anode wires. As a consequence, the field distribution around the wires becomes asymmetric and the gas gain increases in an uncontrollable way. This behavior can be studied by measuring the gas gain along a straw tube between spacers. Probably, the mechanical tension of those straw tubes after their assembly to the frame has been too small. This might

have been caused by an insufficient control of the humidity of the straw material during the gluing process to the Al-frames.

The efficiency distribution of a straw tube as a function of the distance of the track to the anode wire is shown in Fig. 26. The efficiency drops close to the straw walls, where the ionization paths are short due to the cylindrical geometry. The efficiencies are shown for different high voltages. In COMPASS, a HV of 1950 V is used, which corresponds to a gas gain of 6×10^4 . The read-out thresholds were typically set to 6 fC. In the vicinity of the spacers, the efficiency is also reduced as shown in Fig. 27. Fig. 28 shows the drift-times versus the distances of tracks

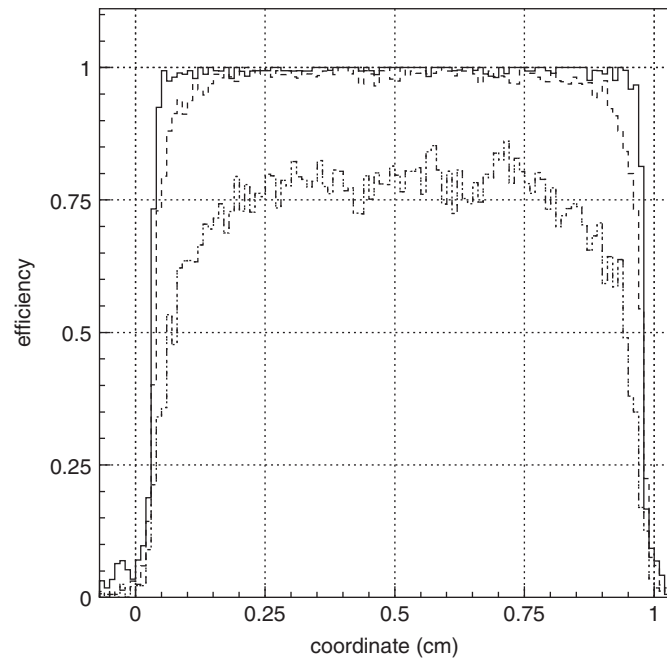


Fig. 26. Efficiency as a function of the coordinate of tracks inside a 10 mm straw tube. The anode wire is situated at 0.5 cm. Three different high voltage settings are shown (solid line: 1950 V, dashed line: 1800 V, dotted line: 1700 V). The threshold was set to 4 fC.

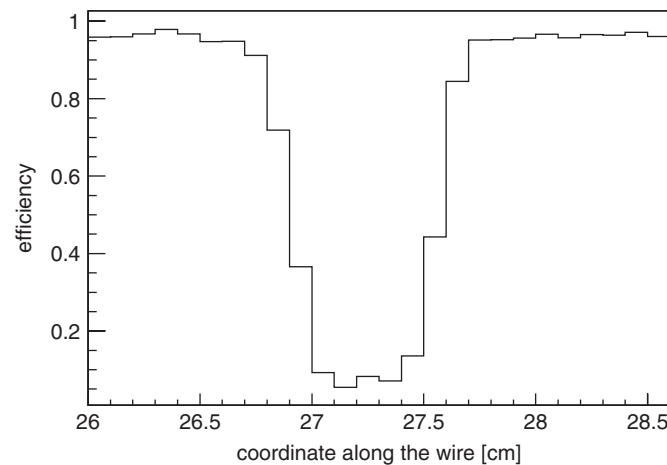


Fig. 27. Efficiency losses along a 6 mm straw in the vicinity of a spacer. The inefficient zone has a size comparable to the straw diameter.

to the anode wire for a typical straw tube (“V-distribution”). Standard tracks, reconstructed by the COMPASS offline analysis (CORAL), were used. The tracks were selected from the central region of the experiment, which is $30 \times 30 \text{ cm}^2$ in size. There, the particle rate was the highest ($> 100,000$ hits/channel/s) and the track reconstruction profits from the high resolution of the COMPASS forward tracking devices like the GEM detectors (resolution $< 70 \mu\text{m}$). By fitting the V-distribution, one obtains the rt-relation, the coordinate $x_{V\text{-fit}}$ of the wire and the time offset t_0 of the TDC-channel. After these free parameters have been fixed, the intrinsic resolution of any individual straw tube can be determined as shown in Fig. 29. A mean resolution of $220 \mu\text{m}$ is achieved, which is slightly worse than the best results from test measurements, which were done with smaller prototypes in the early phase of this project. In order to obtain track coordinates with an absolute precision over the full size of the chamber, which are comparable to the intrinsic resolution of a single straw

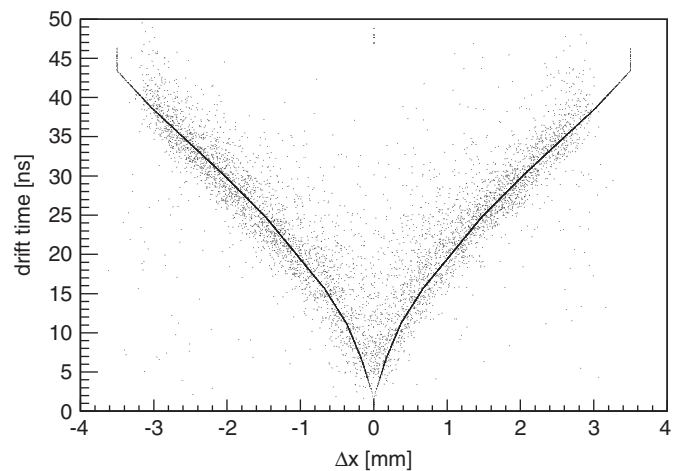


Fig. 28. “V-distribution” of a single wire for particle tracks from 160 GeV muon induced reactions. The full line results from a fit, assuming seven points, between which it is interpolated linearly.

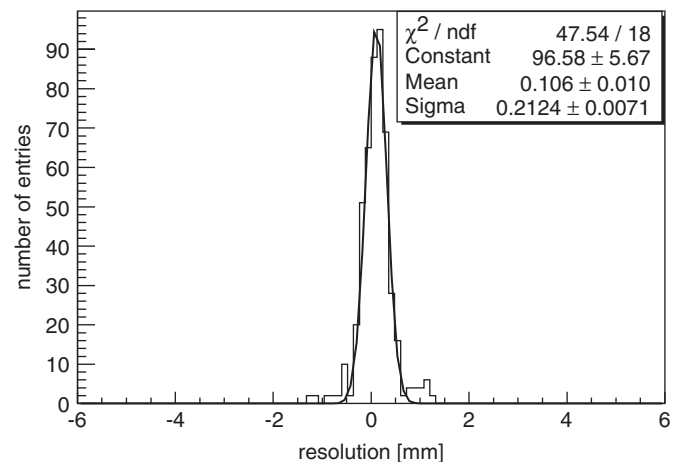


Fig. 29. Residuals of a single wire. The mean resolution is $220 \mu\text{m}$.

(220 μm), two additional corrections have to be applied offline:

1. The geometry correction obtained from the measurements with the X-ray scanner as described in the previous section. This correction accounts for the true zig-zag line of every wire as compared to its position in an idealized homogenous chamber. By applying the X-ray corrections, the uncertainty due to the wire positions is reduced from $\sigma = 180$ to $60 \mu\text{m}$. Combining this uncertainty with the intrinsic resolution of a straw results in a spatial resolution of $230 \mu\text{m}$ for one layer or $230/\sqrt{2} \mu\text{m} \approx 160 \mu\text{m}$ for a double layer.
2. The signal propagation time along a straw: The TDC-values must be corrected for the time, which the signal needs to propagate along a straw. This correction corresponds, over the full length of a straw, to a spatial correction of the order of 1 mm for the drift distances. From the measurements in COMPASS we obtained a propagation velocity of $28.1 \pm 0.6 \text{ cm/ns}$. This is in good agreement with the theoretical value of 27.25 cm/ns , which is expected by the transmission line model described above.

5. Summary and conclusion

The chosen production technology and chamber design allowed the construction of $2.8 \times 3.2 \text{ m}^2$ large tracking chambers with high accuracy, low mass and at a relatively low cost (they are among the largest detectors of their kind). The tracking accuracy is limited by the intrinsic straw drift tube and readout properties on one side and the mechanical precision of the straw tube planes on the other side. Firstly, we obtained a resolution of $220 \mu\text{m}$ per straw while the geometrical precision of wires averaged over all chambers was $170 \mu\text{m}$ (RMS). The best chambers had a geometrical precision of $100 \mu\text{m}$, which seems to be the technological limit for optimized production conditions (humidity, temperature, assembly). Results below $100 \mu\text{m}$ would only be feasible by using straw tubes with a more accurate diameter and using more precise assembly tools. In the present case, the accuracy of the straw's outer diameter was limited by the thickness of the foils, as specified by the producer, while the inner diameter was limited by the straw tube production process.

The limitation of the mechanical precision was overcome by measuring the coordinates of the wires at all spacer

positions with a triple stereo imaging X-ray scanner. Thus, after X-ray correction, a spatial resolution of $160 \mu\text{m}$ per double layer is achieved.

In order to obtain stable operation and the required precision, the chambers have to be operated under stabilized temperature and humidity conditions. The working temperature should stay within $\pm 1 \text{ K}$, in order to avoid further offline corrections. The humidity, under which the chambers should be operated, is defined by the manufacturing technology. In COMPASS the humidity is adjusted to $8 \pm 2\%$.

During 3 years of operation on COMPASS, no symptoms of aging were observed. Only a few straws (less than 1%) were lost due to broken wires.

Acknowledgments

The authors express their gratitude to the Bundesministerium für Bildung und Forschung (BMBF) of Germany, which contributed the largest share, to the JINR and LPP Directorates, and also to their collaboration colleagues for their support and help in the organization of these works. The project was also supported by the Polish Ministry of Science and Information Society Technologies in the frame of two grants: 134/E-365/SPUB-M/CERN/P-03/DZ299/2000 and 134/E-365/SPB/CERN/P-03/DWM 62/2004-2006.

References

- [1] COMPASS. CERN/SPSLC/96-14, SPSLC/P297, 1996.
- [2] ATLAS ID TDR, v.2, CERN/LHCC/97-17, 1997.
- [3] V.N. Bychkov, et al., JINR, E-13-98-269, Dubna, 1998.
- [4] V.N. Bychkov, et al., JINR, E-13-98-209, Dubna, 1998.
- [5] J. Marzec, K. Zaremba, Z. Pawłowski, B. Konarzewski, IEEE Trans. Nucl. Sci. NS-47 (1) (2000) 18.
- [6] J. Marzec, K. Zaremba, Z. Pawłowski, B. Konarzewski, IEEE Trans. Nucl. Sci. NS-49 (2) (2002) 548.
- [7] J. Marzec, Nucl. Instr. and Meth. A 503 (2003) 504.
- [8] V.N. Bychkov, et al., Part. Nucl. Lett. 2 [111] (2002) 64 (Russian journal).
- [9] W. Dünnweber, et al., Nucl. Instr. and Meth. A 515 (2003) 234.
- [10] L. Malter, Phys. Rev. 50 (1936) 48.
- [11] S.N. Gladkikh, et al., Preprint JINR P 13-2001-275, Dubna, 2001.
- [12] B. Howell, D. Koltick, M. Kobayashi, Nucl. Instr. and Meth. A 289 (1990) 185.
- [13] R.E. Avery, et al., IEEE Trans. Nucl. Sci. NS-40 (1993) 578.
- [14] K. Platzer, W. Dünnweber, H. Wellenstein, IEEE Trans. Nucl. Sci. NS-51 (4) (2004) 1555.
- [15] K. Platzer, et al., IEEE Trans. Nucl. Sci. NS-52 (3) (2005) 793.